INTERNATIONAL JOURNAL FOR NUMERICAL METHODS IN FLUIDS
Int. J. Numer. Meth. Fluids 2006; **51**:1277–1296
Published online 28 December 2005 in Wiley InterScience (www.interscience.wiley.com). DOI: 10.1002/fld.1153

Improvements in mass conservation using alternative boundary implementations for a quasi-bubble finite element shallow water model

Shintaro Bunya[1,*,†], Shinobu Yoshimura[2] and Joannes J. Westerink[1]

[1]*Department of Civil Engineering and Geological Sciences, University of Notre Dame, Notre Dame, IN 46556, U.S.A.*
[2]*Institute of Environmental Studies, The University of Tokyo, 7-3-1 Hongo, Bunkyo, Tokyo 113-8656, Japan*

SUMMARY

Finite element approaches generally do not guarantee exact satisfaction of conservation laws especially when Dirichlet-type boundary conditions are imposed. This article discusses improvement of the global mass conservation property of quasi-bubble finite element solutions for the shallow water equations, focusing on implementations of the surface-elevation boundary conditions. We propose two alternative implementations, which are shown by numerical verification to be effective in improving the smoothness of solutions near the boundary and in reducing the mass conservation error. The improvement of the mass conservation property contributes to augmenting the reliability and robustness of long-term time integrations. Copyright © 2006 John Wiley & Sons, Ltd.

KEY WORDS: shallow water equations; boundary conditions; conservation laws; quasi bubble-function element; finite element method

1. INTRODUCTION

Finite element solutions to the shallow water equations (SWE) have been successfully used to model ocean flow problems such as tides and the propagation of storm surges and tsunami-waves. On the other hand, in solving long-term coupled flow-transport phenomena such as

*Correspondence to: Shintaro Bunya, Department of Civil Engineering and Geological Sciences, University of Notre Dame, Notre Dame, IN 46556, U.S.A.
†E-mail: sbunya@nd.edu

Received 21 July 2005
Revised 17 October 2005
Accepted 18 October 2005

sediment transport and marine ecosystem dynamics, the finite difference and finite volume methods tend to be preferred. One of the major reasons why the finite element method is avoided is that exact satisfaction of mass conservation is not guaranteed. Even a small amount of error in mass conservation may not be acceptable when a long-term time integration is involved and the accumulation of the error is significant.

When one examines the mass conservation property of a finite element scheme, it may mean either one of the two different scales of conservation: local or global conservation. The former, local conservation is frequently noted when one emphasizes the superiority of the control volume method or finite volume method, which readily conserve conservative quantities cell by cell. On the other hand, it is often said that the finite element method is not locally conservative. This statement may be true in case that element-wise conservation of mass or other conservative quantities must be achieved. However, according to Huges *et al.* [1], the finite element method is locally conservative if one is satisfied with a node-by-node conservation. Further, they argued that an element-wise conservation is also achievable by a deliberate post-processing.

With respect to the global conservation property, it is often considered that the finite element method should readily satisfy the global conservation properly. However, this is not necessarily true when a Dirichlet-type boundary condition is involved [1]. This is because, in the conventional implementation of the Dirichlet-type boundary conditions, discrete nodal conservation laws are replaced with the specified boundary condition; and thus the solution may not satisfy the prescribed conservation law. This is related to the space of the test function ordinarily used, which vanishes on the Dirichlet boundary. The focus of this article is on improving the mass conservation property by introducing alternative implementations of the Dirichlet-type boundary conditions.

We have developed a software system to solve the SWE using the finite element method. While many finite element formulations have been investigated in order to eliminate spurious oscillation in finite element fluid analyses [2–9], we have adopted a quasi bubble-function approach, which was introduced by Mewis and Holz [10] to the SWE and extensively used in the TELEMAC model [11, 12] developed by Electricité de France (EDF). Atkinson *et al.* [13] showed that the quasi bubble-function finite element model is equivalent to an optimal form of the generalized wave continuity equation model, which has also been extensively exercised in practical use [9].

While this mixed finite element formulation using linear and quasi bubble-function elements shows very good stability in the interior domain, our early work demonstrated that the quasi-bubble scheme leads to a significant instability when a surface-elevation boundary condition is implemented as an essential boundary condition [14]. In the same article, we proposed an alternative implementation called the 'discontinuous boundary implementation' (DBI). The alternative implementation was found to be effective to remedy the instability related to the surface-elevation boundary condition in 1-D cases.

In this article, we extend the DBI for 2-D cases. We rename it the 'discontinuous velocity boundary implementation' (DVBI) for convenience. In addition, we propose another alternative formulation, which is called the 'discontinuous surface-elevation boundary condition' (DSBI) in this article. After the alternative formulations are introduced, numerical experiments are presented. From the numerical experiments, it is indicated that these alternative implementations are also effective in improving the mass conservation property in addition to improving the stability of the computations.

2. GOVERNING EQUATIONS AND FINITE ELEMENT APPROXIMATION

The two-dimensional SWE are written as

$$\frac{\partial \zeta}{\partial t} + \frac{\partial H u_i}{\partial x_i} = 0 \tag{1}$$

$$\frac{\partial u_i}{\partial t} + u_j \frac{\partial u_i}{\partial x_j} + g \frac{\partial \zeta}{\partial x_i} + \tau u_i + f_i = 0 \tag{2}$$

where indexes $i \in \{1,2\}$ and $j \in \{1,2\}$ represent the horizontal Cartesian coordinate, ζ is the surface elevation, $H = h + \zeta$ is the total water depth, h is the bathymetric depth, u_i is the horizontal velocity field, g is the gravitational acceleration, τ is the bottom friction coefficient. The Coriolis force, surface wind stress, variable atmospheric pressure, tidal potential, horizontal turbulent viscosity are incorporated into the body force f_i. Equation (1) is the continuity equation in primitive form, and Equation (2) is the momentum equation in non-conservative form. The summation rule is implied.

Let Γ_S denote the open boundary, where a surface elevation is specified by a prescribed value $\hat{\zeta}$ as

$$\zeta = \hat{\zeta} \tag{3}$$

This surface-elevation boundary condition is often imposed to propagate tides from the open ocean into the domain and is generally referred to as an open boundary. In this article, we focus on various implementation of the open ocean boundary conditions. This very energetic boundary conditions exhibit poor local accuracy, large mass conservation errors and significant stability problems.

Let Γ_L and Γ_S be partitions of domain boundary Γ. Let Γ_L denote the land boundary defined as

$$\mathbf{u} \cdot \mathbf{n} = 0 \tag{4}$$

which represents no normal flow.

Letting ζ^* and u_i^* be test functions for the continuity and momentum equations, respectively, we have the following weighted residual statements of the governing equations:

$$\int \zeta^* \left(\frac{\partial \zeta}{\partial t} + \frac{\partial H u_i}{\partial x_i} \right) \mathrm{d}\Omega = 0 \tag{5}$$

$$\int u_i^* \left(\frac{\partial u_i}{\partial t} + u_j \frac{\partial u_i}{\partial x_j} + g \frac{\partial \zeta}{\partial x_j} + \tau u_i + f_i \right) \mathrm{d}\Omega = 0 \tag{6}$$

To obtain the matrix forms of the weighted residual equations, the unknown functions and test functions are expanded with finite element bases. We adopt a mixed interpolation to avoid spurious modes. Specifically, the surface elevation ζ and the test function ζ^* is interpolated with the standard triangular linear element, and the velocity u_i and the test function u_i^* is interpolated with a triangular quasi bubble-function element. This type of mixed interpolation

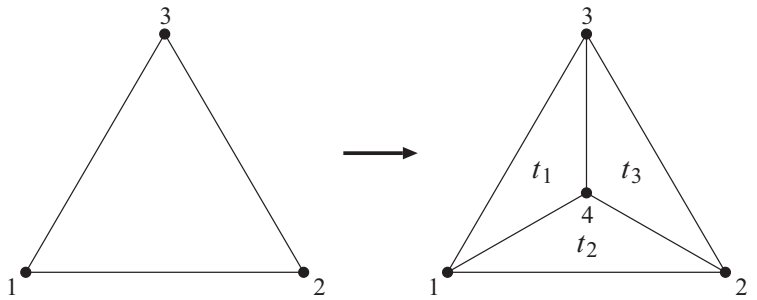

Figure 1. Sub-division of a triangle with a centroid node.

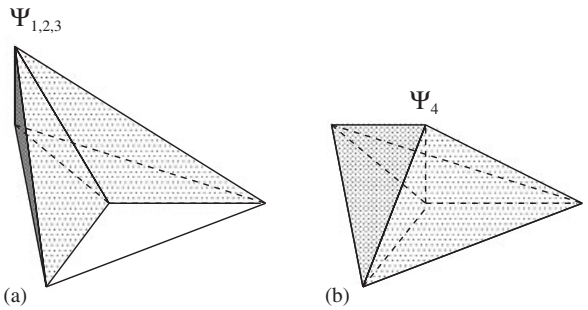

Figure 2. Finite element bases of a quasi-bubble element: (a) basis for a standard node; and (b) basis for a quasi-bubble node.

are introduced by Mewis and Holz [10] to the SWE, and was demonstrated to effectively remove spurious oscillations. The quasi bubble-function element has a centroid node in addition to three nodes at each corner of a triangle. The centroid node divides a triangle into three sub-triangles as shown in Figure 1. Letting each sub-triangle be a standard linear element, a quasi-bubble element has piecewise linear bases shown in Figure 2. Thus ζ and ζ^* are expanded with the linear elements as

$$\zeta = \sum_{\alpha=1}^{N} \zeta_\alpha \phi_\alpha \quad \text{and} \quad \zeta^* = \sum_{\alpha=1}^{N} \zeta_\alpha^* \phi_\alpha \tag{7}$$

where α is a nodal index, N is the number of corner nodes, and ζ_α and ζ_α^* are nodal coefficients. On the other hand, u_i and u_i^* are expanded with the quasi-bubble elements as

$$u_i = \sum_{\beta=1}^{M} u_{i\beta} \psi_\beta \quad \text{and} \quad u_i^* = \sum_{\beta=1}^{M} u_{i\beta}^* \psi_\beta \tag{8}$$

where $u_{i\beta}$ and $u_{i\beta}^*$ are nodal unknowns, and M is the number of the corner and centroid nodes.

By expanding the test functions and considering their arbitrariness, Equations (5) and (6) yield the following nodal equations:

$$\int_\Omega \frac{\partial \zeta}{\partial t}\phi_\alpha \,\mathrm{d}\Omega + \int_\Omega \frac{\partial H u_i}{\partial x_i}\phi_\alpha \,\mathrm{d}\Omega = 0 \tag{9}$$

$$\int_\Omega \frac{\partial u_i}{\partial t}\psi_\beta \,\mathrm{d}\Omega + \int_\Omega u_j \frac{\partial u_i}{\partial x_j}\psi_\beta \,\mathrm{d}\Omega + \int_\Omega g\frac{\partial \zeta}{\partial x_i}\psi_\beta \,\mathrm{d}\Omega + \int_\Omega \tau u_i \psi_\beta \,\mathrm{d}\Omega + \int_\Omega f_i \psi_\beta \,\mathrm{d}\Omega = 0 \tag{10}$$

Unknown variables ζ and u_i are not expanded for convenience of the following discussion.

An explicit two-step finite difference scheme is adopted to discretize the time derivative terms [15]. In order to minimize phase errors we use the consistent mass matrix in both the left- and right-hand sides, instead of using a lumped mass matrix for speed-up.

3. IMPLEMENTATIONS OF BOUNDARY CONDITIONS

Our early work demonstrated that the quasi-bubble approach yields an erroneous solution when a Dirichlet-type boundary condition of surface elevation, defined in Equation (3), is implemented in a conventional manner [14]. Special attention should be paid to this boundary condition since it is often used to propagate tides into gulfs or bays and the accuracy of global mass conservation largely depends on a quality of solution on the boundary. We proposed an alternative implementation of the surface-elevation boundary condition and tested it in a one-dimensional problem [14]. In this article, we extend this paradigm to a two-dimensional form. In addition, we propose another alternative implementation of the boundary condition.

3.1. Discontinuous velocity boundary implementation

We introduced an alternative implementation of the surface-elevation boundary condition in [14] and called it a DBI because it allows a numerical solution to have dual velocity values at each node on Γ_S. We here extend it into a two-dimensional form and rename it a DVBI to differentiate it from another alternative formulation, which we propose in the next section.

3.1.1. Derivation. Applying integration by parts to the first-order spatial derivative in Equation (9), we obtain

$$\int_\Omega \frac{\partial \zeta}{\partial t}\phi_\alpha \,\mathrm{d}\Omega - \int_\Omega H u_i \frac{\partial \phi_\alpha}{\partial x_i}\,\mathrm{d}\Omega + \int_\Gamma \phi_\alpha H u_i n_i \,\mathrm{d}\Gamma = 0 \tag{11}$$

Further, Equation (10) may have an alternative form by applying integration by parts to the advection term:

$$\begin{aligned}\int_\Omega u_j \frac{\partial u_i}{\partial x_j}\psi_\beta \,\mathrm{d}\Omega &= -\int_\Omega u_i \frac{\partial u_j \psi_\beta}{\partial x_j}\,\mathrm{d}\Omega + \int_\Gamma \psi_\beta u_i u_j n_j \,\mathrm{d}\Gamma \\ &= -\int_\Omega u_i u_j \frac{\mathrm{d}\psi_\beta}{\mathrm{d}x_j}\,\mathrm{d}\Omega - \int_\Omega u_i \frac{\partial u_j}{\partial x_j}\psi_\beta \,\mathrm{d}\Omega + \int_\Gamma \psi_\beta u_i u_j n_j \,\mathrm{d}\Gamma\end{aligned} \tag{12}$$

Then, we have an alternative form of the momentum equation:

$$\int_\Omega \frac{\partial u_i}{\partial t}\psi_\beta \,\mathrm{d}\Omega - \int_\Omega u_i u_j \frac{\mathrm{d}\psi_\beta}{\mathrm{d}x_j}\,\mathrm{d}\Omega - \int_\Omega u_i \frac{\partial u_j}{\partial x_j}\psi_\beta \,\mathrm{d}\Omega + \int_\Omega g\frac{\partial \zeta}{\partial x_i}\psi_\beta \,\mathrm{d}\Omega + \int_\Omega \tau u_i \psi_\beta \,\mathrm{d}\Omega + \int_\Omega f_i \psi_\beta \,\mathrm{d}\Omega + \int_\Gamma \psi_\beta u_i u_j n_j \,\mathrm{d}\Gamma = 0 \tag{13}$$

We assume that the normal component of velocity, i.e. $u_\mathrm{n} \equiv u_j n_j$, in the boundary integral may be defined as external and is an additional unknown independent of the internal unknowns. Denoting an external normal component of velocity by $\hat{u}_\mathrm{n}$ and letting $\hat{Q}_\mathrm{n} \equiv H\hat{u}_\mathrm{n}$, Equations (11) and (13) may be rewritten as

$$\int_\Omega \frac{\partial \zeta}{\partial t}\phi_\alpha \,\mathrm{d}\Omega - \int_\Omega H u_i \frac{\partial \phi_\alpha}{\partial x_i}\,\mathrm{d}\Omega + \int_\Gamma \phi_\alpha \hat{Q}_\mathrm{n}\,\mathrm{d}\Gamma = 0 \tag{14}$$

and

$$\int_\Omega \frac{\partial u_i}{\partial t}\psi_\beta \,\mathrm{d}\Omega - \int_\Omega u_i u_j \frac{\mathrm{d}\psi_\beta}{\mathrm{d}x_j}\,\mathrm{d}\Omega - \int_\Omega u_i \frac{\partial u_j}{\partial x_j}\psi_\beta \,\mathrm{d}\Omega + \int_\Omega g\frac{\partial \zeta}{\partial x_i}\psi_\beta \,\mathrm{d}\Omega + \int_\Omega \tau u_i \psi_\beta \,\mathrm{d}\Omega + \int_\Omega f_i \psi_\beta \,\mathrm{d}\Omega + \int_\Gamma \psi_\beta u_i \hat{u}_\mathrm{n} \,\mathrm{d}\Gamma = 0 \tag{15}$$

3.1.2. Open boundary Γ_S. On open boundaries, surface elevation is specified by Equation (3). In the conventional approach, Equation (3) is imposed in strong form, and nodal continuity equations on Γ_S are eliminated from a set of simultaneous equations. By contrast, as demonstrated later, the DVBI being presented utilizes the nodal equations to obtain $\hat{Q}_\mathrm{n}$, which is a boundary flux viewed as external to the domain, i.e. an added unknown quantity. The additional unknown function $\hat{Q}_\mathrm{n}$ can be determined on Γ_S if Equation (14) is solved with respect to $\hat{Q}_\mathrm{n}$ as follows:

$$\int_{\Gamma_\mathrm{S}} \hat{Q}_\mathrm{n}\phi_\alpha \,\mathrm{d}\Gamma = -\int_\Omega \frac{\partial \zeta}{\partial t}\phi_\alpha \,\mathrm{d}\Omega + \int_\Omega H u_i \frac{\mathrm{d}\phi_\alpha}{\mathrm{d}x_i}\,\mathrm{d}\Omega \tag{16}$$

because ζ in the right-hand side is not unknown on Γ_S but prescribed by Equation (3) as a boundary condition. Similar formulations have been introduced by Lynch and Gray [16] and Kolar *et al.* [17] for the wave equation model [9, 16]. Lynch and Gray [16] suggested solving the wave equation for $\hat{Q}_\mathrm{n}$ to determine the normal component of velocity, and to solve the tangential component of the momentum equation to obtain the tangential component of velocity. (In contrast, the DVBI approach modifies only the advection term as explained later.) Kolar *et al.* [17] used Equation (16) as a post-processing step; they solved for $\hat{Q}_\mathrm{n}$ to give perfectly mass-conserving flux. (On land boundaries, they used the same equation to determine ζ, enforcing no normal flow with $\hat{Q}_\mathrm{n} = 0$.)

Guided by their work, we utilize the auxiliary flux, $\hat{Q}_\mathrm{n}$, to remedy the instability that arises with the surface-elevation boundary condition for quasi-bubble solutions to the SWE

[14]. Using $\hat{Q}_n$ solved with Equation (16) we obtain $\hat{u}_n$, which is the normal component of velocity on Γ_S viewed as external to the domain. Since H on Γ_S has been determined by the boundary condition, $\hat{u}_n$ is readily obtained as follows:

$$\hat{u}_n = \frac{\hat{Q}_n}{H} \tag{17}$$

Because we found in Reference [14] that Equation (17) needs to be upstreamed to improve stability, instead of using Equation (17) we use

$$\hat{u}_n = \begin{cases} \dfrac{\hat{Q}_n}{H}, & \hat{Q}_n < 0 \text{ (inflow)} \\ u_n, & \hat{Q}_n \geqslant 0 \text{ (outflow)} \end{cases} \tag{18}$$

Then $\hat{u}_n$ is utilized by substituting it into Equation (15). We hypothesize that the newly obtained $\hat{u}_n$, which is solved from the nodal continuity equation should improve the accuracy of solution near the boundary. This is confirmed by numerical experiments presented later.

3.1.3. Land boundary Γ_L. The land boundaries, which are defined as no normal flow boundaries by Equation (4), are implemented in this article by setting the normal component of velocity equal to zero after performing a normal–tangential coordinate transformation. Thus the land boundary is implemented as an essential boundary condition in a conventional way. Note that the boundary integration terms in Equations (14) and (15) equal zero on Γ_L since $\hat{u}_n = 0$ and $\hat{Q}_n = 0$ according to Equation (4).

3.2. Discontinuous surface-elevation boundary implementation

A DSBI is introduced in this section as another effective formulation to implement the surface-elevation boundary condition with improved accuracy. The derivation of the DSBI also starts with an integration by parts procedure. This time, the integration by parts is applied to the spatial derivative of ζ in Equation (10). Then we have

$$\int_\Omega \frac{\partial u_i}{\partial t}\psi_\beta \,\mathrm{d}\Omega + \int_\Omega u_j \frac{\partial u_i}{\partial x_j}\psi_\beta \,\mathrm{d}\Omega - \int_\Omega \zeta \frac{\mathrm{d}\psi_\beta}{\mathrm{d}x_i}\,\mathrm{d}\Omega + \int_\Omega \tau u_i, \psi_\beta \,\mathrm{d}\Omega + \int_\Omega f_i, \psi_\beta \,\mathrm{d}\Omega + \int_\Gamma \hat{\zeta}\psi_\beta n_i \,\mathrm{d}\Gamma = 0 \tag{19}$$

where Equation (3) is substituted in the boundary integration term.

3.2.1. Open boundary Γ_S. We impose the surface-elevation boundary condition in weak form by using the boundary integration term in Equation (19). Because of the weak enforcement of the boundary condition, the computed surface elevation ζ on Γ_S may differ from the prescribed boundary value $\hat{\zeta}$. Thus we call this alternative form of the surface-elevation boundary condition a discontinuous surface-elevation boundary condition, due to the discontinuity between ζ and $\hat{\zeta}$ on Γ_S.

Our numerical experiments indicate that, the discontinuity between ζ and $\hat{\zeta}$ sometimes become too large to have a stable solution. In order to control the size of the discontinuity, or jump, a jump-control term can be added to the continuity equation. The resulting modified continuity equation is written as

$$\int_{\Omega} \frac{\partial \zeta}{\partial t} \phi_\alpha \, \mathrm{d}\Omega + \int_{\Omega} \frac{\partial H u_i}{\partial x_i} \phi_\alpha \, \mathrm{d}\Omega + \int_{\Gamma_S} \tau_d (\zeta - \hat{\zeta}) = 0 \tag{20}$$

where τ_d is a coefficient with which the amount of the jump can be controlled. A similar idea to this additional term has been applied with the discontinuous Galerkin method [18]. When τ_d is very large, the jump control term works as penalty in the penalty method. However, in our cases, it was observed that τ_d can take a small value relative to the coefficient matrix terms associated with $\partial\zeta/\partial t$. Thus the boundary integration term in Equation (19) is substantially used to enforce the surface-elevation boundary condition in a weak sense and the jump control term is for supplemental use.

3.2.2. Land boundary Γ_L. The land boundary defined by Equation (4) is implemented in the same way as in the DVBI; it is implemented as an essential boundary condition in a conventional way after coordinate transformation.

4. NUMERICAL VERIFICATION

The proposed alternative formulations are examined in this section by solving Lynch and Gray's quarter-annulus test problem with quadratically varying bathymetry [19]. The following three cases are solved for specific purposes:

Case a: A linearized quarter-annulus problem, in which numerical solutions are compared with the theoretical analytical solution derived by Lynch and Gray [19].
Case b: A non-linear quarter-annulus problem, in which the global mass conservation property under a axis symmetric condition is examined.
Case c: A non-linear quarter-annulus problem with the Coriolis force, in which the global mass conservation property under an asymmetric condition is examined.

The geometry is depicted in Figure 3. The inner radius r_1 is set to 2×10^5 ft (60.96 km), and the outer radius r_2 is 5×10^5 ft (152.4 km). Bathymetry varies quadratically between $h = 10$ ft (3.048 m) at r_1 and $h = 62.5$ ft (19.05 m) at r_2. The linear bottom friction is adopted with the coefficient τ of $0.0001\,\mathrm{s}^{-1}$. Δt is set to 12.5 s and 0.01. The coefficient of the jump control term, τ_d, is set to 0.01. An M_2 tidal wave with the amplitude of 1.0 ft (0.3048 m) is imposed on the seaward boundary as a surface-elevation boundary condition. The grid used in this test is shown in Figure 4.

4.1. Case a: a linearized quarter-annulus test problem

The quarter-annulus test problem was solved with the linearized SWE, which are written as

$$\frac{\partial \zeta}{\partial t} + \frac{\partial h u_i}{\partial x_i} = 0 \tag{21}$$

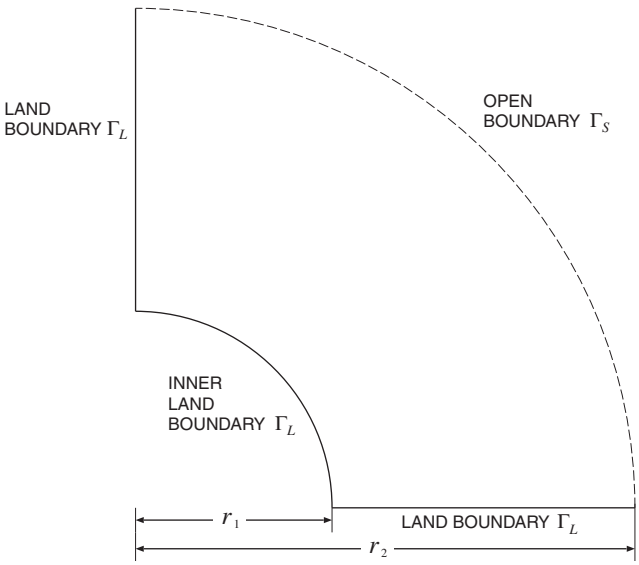

Figure 3. Geometry and boundaries for the quarter-annulus test problem.

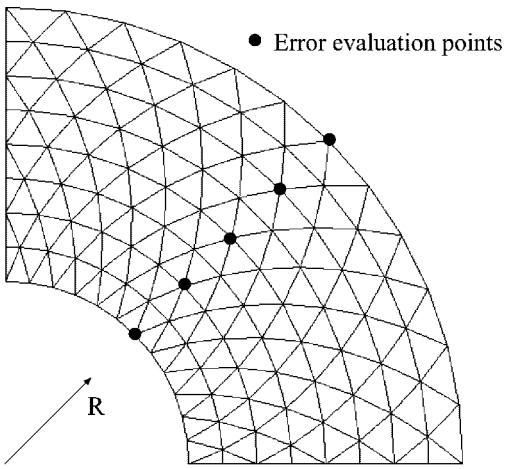

Figure 4. Triangular grid for the quarter-annulus test problem. In Case a, numerical solutions are compared with the theoretical exact solution at the marked nodes.

$$\frac{\partial u_i}{\partial t} + g\frac{\partial \zeta}{\partial x} + \tau u_i = 0 \tag{22}$$

where τ is constant. The numerical results are compared with the exact analytical solution. Figures 5 and 6 show the error in surface elevation ζ and radial velocity u_r, respectively.

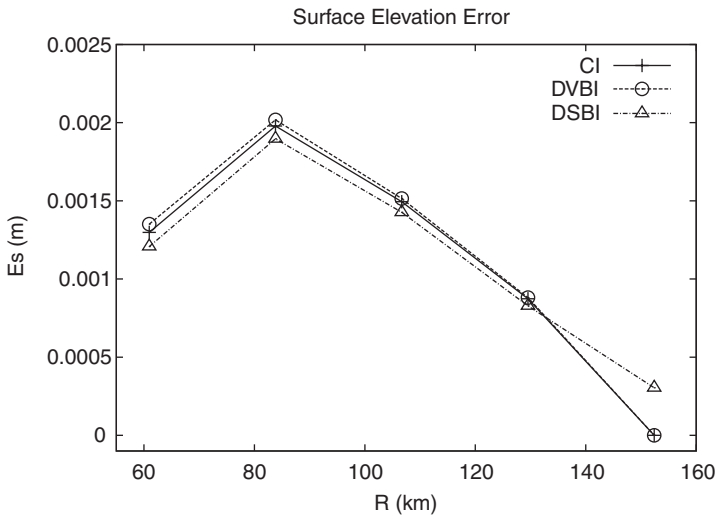

Figure 5. Error profile of the surface elevation for Case a. The error is evaluated as a maximum discrepancy of numerical solutions from the analytical solution during the tenth period.

The error plotted in the figures is defined at each error evaluation node as

$$E_s = \max |\zeta^n - \zeta^a| \text{ in the tenth tidal cycle} \tag{23}$$

$$E_v = \max |u_r^n - u_r^a| \text{ in the tenth tidal cycle} \tag{24}$$

where ζ^n and u_r^n represent the computed surface elevation and radial velocity component while ζ^a and u_r^a are the corresponding analytical solutions. In the figures, the CI stands for the conventional implementation, with which the surface-elevation boundary condition is implemented in strong form. We note in Figure 5 that the DSBI yields a slightly better solution than the CI at interior nodes in spite of the fact that the DSBI solution does not exactly meet the prescribed boundary condition at the open boundary node. With respect to the DVBI solution, it does not improve the solution, or it has an even larger error than the CI. This is however not an unexpected result as long as the increase of the error is small since that the DVBI scheme is only effective in conjunction with the advection terms, which are not included in the linearized form of the SWE described in Equations (21) and (22).

A more evident distinction is observed in the velocity error. Figure 6 shows that the CI and DVBI locally yield a large discrepancy in velocity at the open boundary node. On the other hand, the error profile of the DSBI solution is smooth near the boundary. An erroneous solution on the boundary may deteriorate global mass conservation. Figure 7 shows the error in the numerical boundary flux. The error E_{BF} is defined as

$$E_{BF}(t) = -\int_{\Gamma_S} H(t) u_r(t)\, d\Gamma - \frac{d}{dt}\int_{\Omega} \zeta(t)\, d\Omega \tag{25}$$

The first term on the right-hand side represents the instantaneous inflow through Γ_S and the second term represents the volume increase rate over the whole domain. Thus the difference

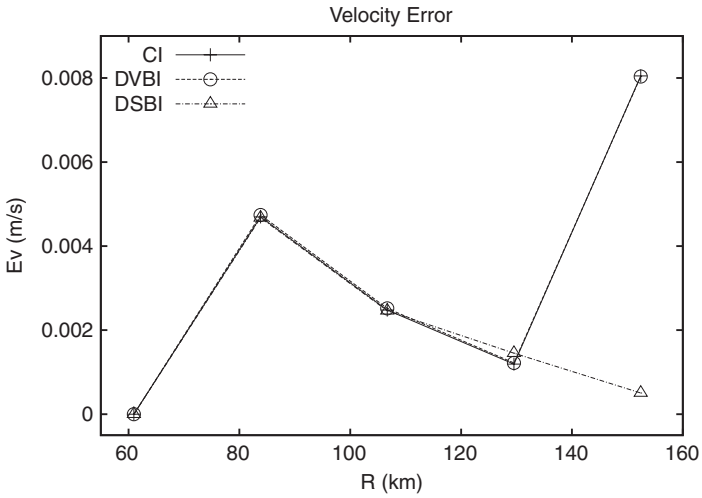

Figure 6. Error profile of the radial velocity for Case a. The error is evaluated as a maximum discrepancy of numerical solutions from the analytical solution during the tenth period.

E_{BF} should be zero if a numerical solution holds an exact value. In Figure 7, the CI and DVBI show the same level of error, while the DSBI yields much smaller errors. In order to see the accumulation of the boundary flux error, we plotted ΔV_Ω and ΔV_{Γ_s} in Figures 8–10. The ΔV_Ω and ΔV_{Γ_s} are defined as

$$\Delta V_\Omega(t) = \int_\Omega \zeta(t)\,\mathrm{d}\Omega - \int_\Omega \zeta(0)\,\mathrm{d}\Omega \tag{26}$$

$$\Delta V_{\Gamma_s}(t) = -\int_0^t \int_{\Gamma_s} H(t')u_r(t')\,\mathrm{d}\Gamma\,\mathrm{d}t' \tag{27}$$

Thus ΔV_Ω and ΔV_{Γ_s} should be identical when an exact solution is obtained. Comparing Figures 8 and 9, no distinction is observed. Again, this is an expected result because the DVBI is effective only when the advection terms are active. While a small discrepancy in cumulative mass conservation is observed for the CI and DVBI solutions in both Figures 8 and 9, the DSBI solutions shows an excellent cumulative mass conservation accuracy in Figure 10.

4.2. Case b: a non-linear quarter-annulus problem without the Coriolis force

In this case, we examine mass conservation properties with the non-linear SWE. Since the Coriolis effect is not included, the solution ought to be axially symmetric.

The error in the boundary flux defined in Equation (25) is plotted in Figure 11, which shows that the CI solution yields the most erroneous boundary flux, the DVBI solution reduces the error to a considerable extent, and the DSBI solution extensively improves the mass balance. While the effectiveness of the DSBI is very evident, that of the DVBI is not outstanding. However, an important improvement can be found if one notices the symmetry of the positive and negative portions of the mass imbalance errors. Denoting the amplitude of E_{BF} in the positive side by A_+ and that in the negative side by A_-, it is observed that A_+ is quite different

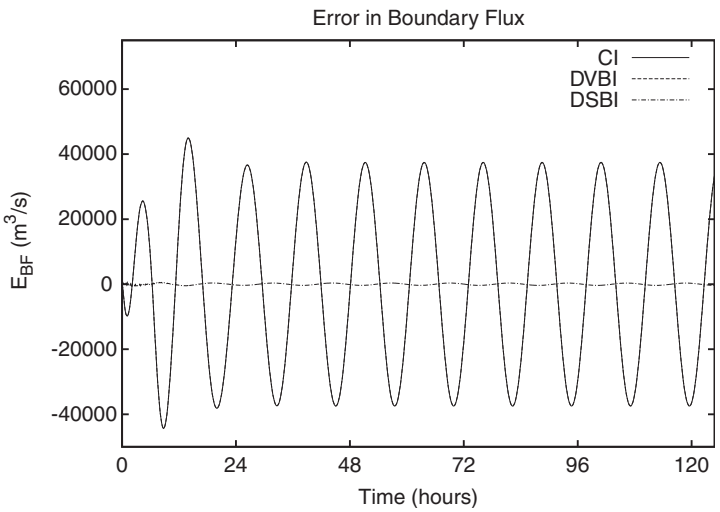

Figure 7. Comparison of the discrepancy between inflows through the open boundary and the water volume increase rate in the computational domain (Case a).

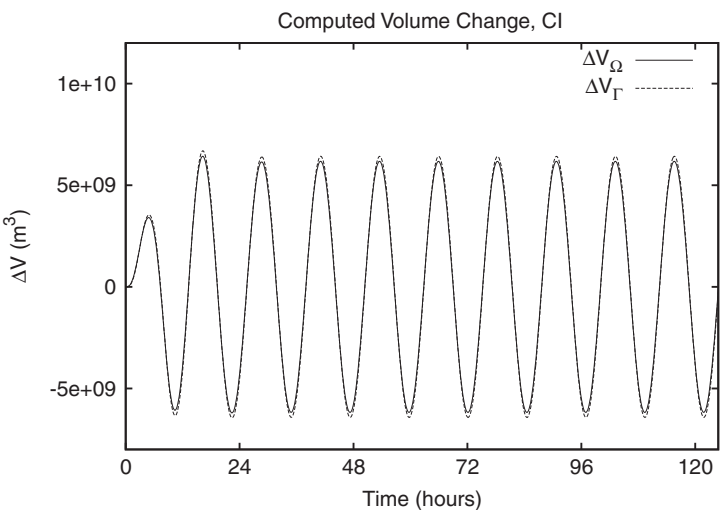

Figure 8. Volume increase calculated with the CI solution. The solid line was obtained with the domain integral of the surface-elevation term. The dashed line was obtained with the boundary integral of the flux through Γ_S (Case a).

from A_- in the CI solution while A_+ balances A_- in the DSBI solution. The symmetric distribution of the error in the DSBI solution is preferable because the positive and negative parts cancel each other out. This results in a small accumulation of the mass error, which is clearly observed in Figure 13.

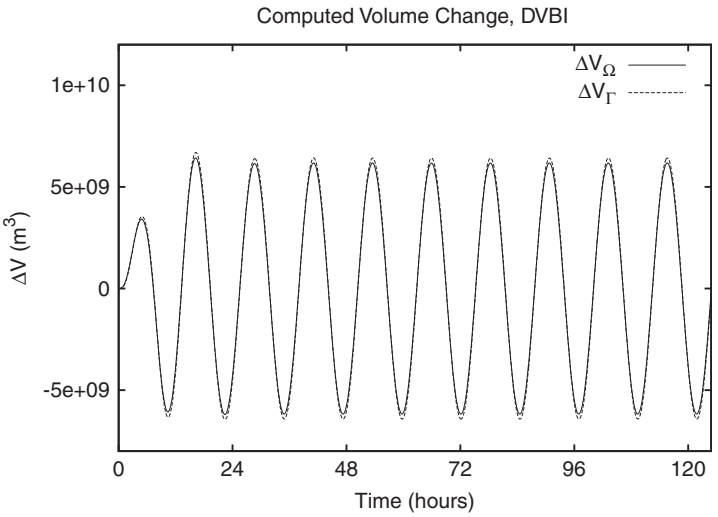

Figure 9. Volume increase calculated with the DVBI solution. The solid line was obtained by domain integral of the surface-elevation term. The dashed line was obtained with the boundary integral of the flux through Γ_S (Case a).

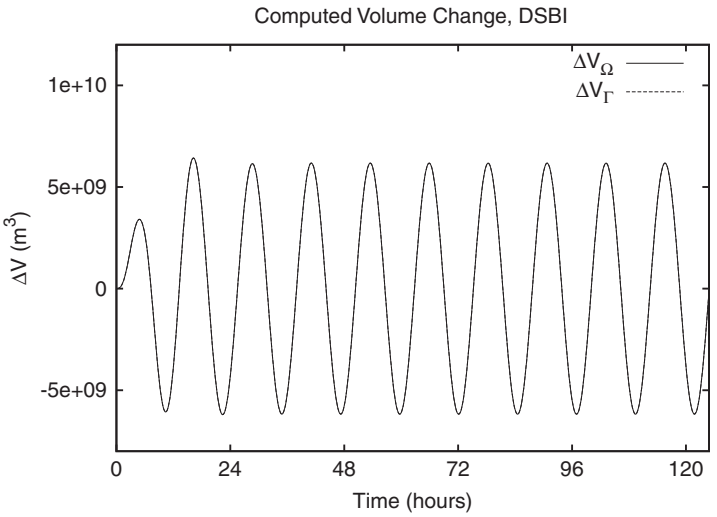

Figure 10. Volume increase calculated with the DSBI solution. The solid line was obtained with the domain integral of the surface-elevation term. The dashed line was obtained with the boundary integral of the flux through Γ_S (Case a).

Figure 12 shows a global mass conservation error in the CI solution. The error is linearly accumulating as time proceeds. On the other hand, the error does not seem to be accumulating for the DVBI solution scheme in Figure 13. With respect to the DSBI solution, Figure 14 shows its excellent mass conservation property.

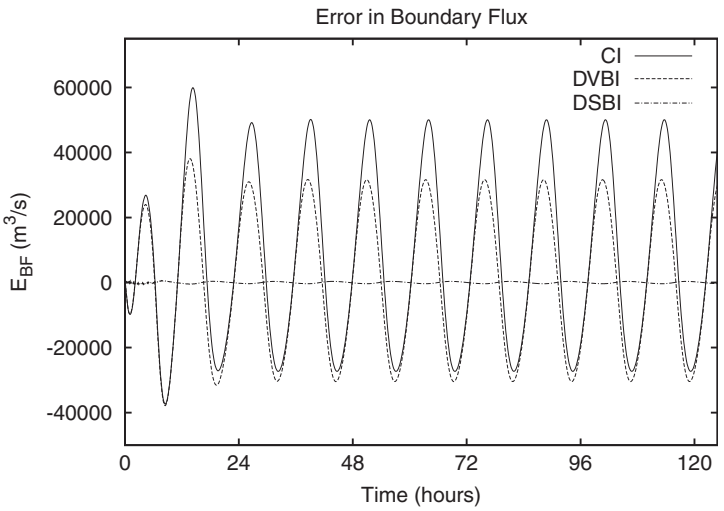

Figure 11. Comparison of the discrepancy between inflows through the open boundary and the water volume increase rate in the computational domain (Case b).

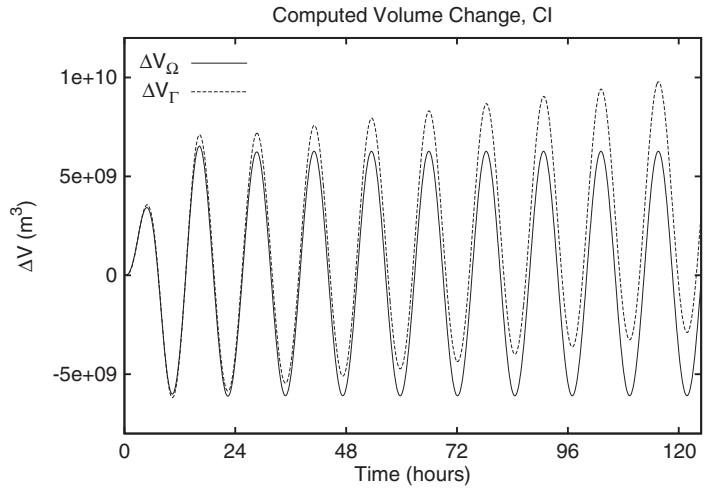

Figure 12. Volume increase calculated with the CI solution. The solid line was obtained with the domain integral of the surface-elevation term. The dashed line was obtained with the boundary integral of the flux through Γ_S (Case b).

4.3. Case c: a non-linear quarter-annulus test problem with the Coriolis force

In this case, in order to examine the proposed boundary implementation in an axially asymmetric condition, the Coriolis term is added to the governing equations used in Case b.

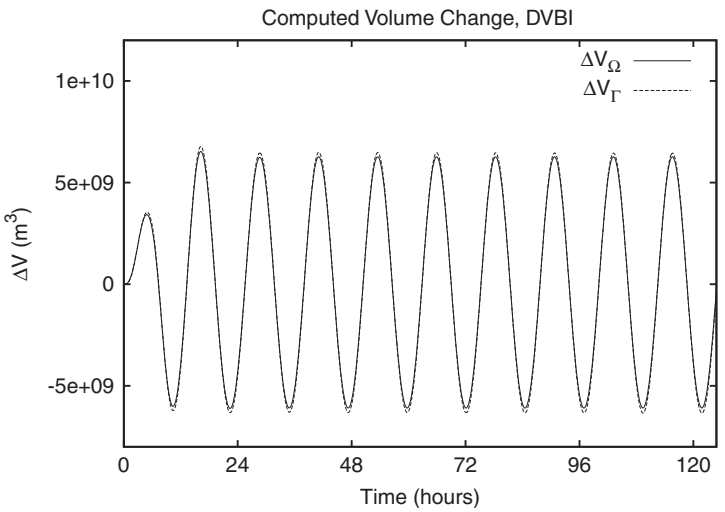

Figure 13. Volume increase calculated with the DVBI solution. The solid line was obtained with the domain integral of the surface-elevation term. The dashed line was obtained with the boundary integral of the flux through Γ_S (Case b).

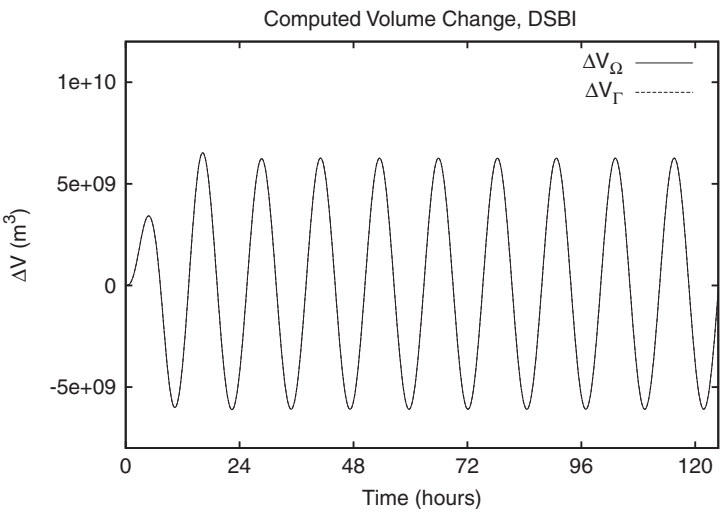

Figure 14. Volume increase calculated with the DSBI solution. The solid line was obtained with the domain integral of the surface-elevation term. The dashed line was obtained with the boundary integral of the flux through Γ_S (Case b).

The boundary flux error, E_{BF}, defined in Equation (25) is plotted in Figure 15. The trend of the amount of mass error is the same as that of Case b, shown in Figure 11. However, the positive–negative asymmetry of the mass error profile seems to be reduced for the CI solution,

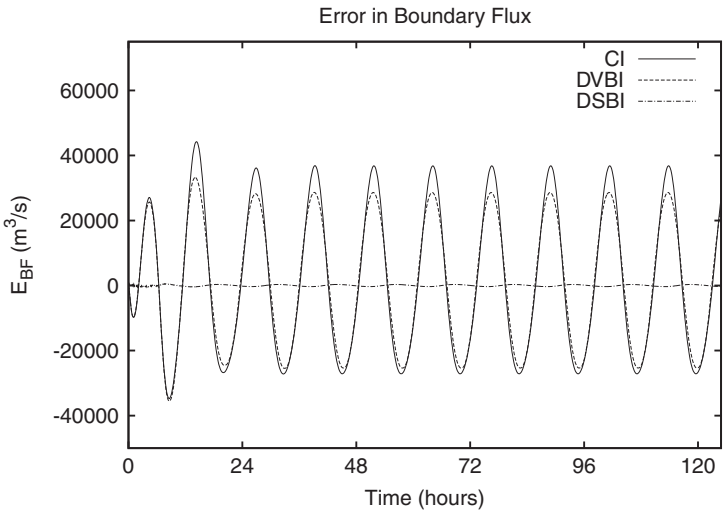

Figure 15. Comparison of the discrepancy between inflows through the open volume increase rate in the computational domain (Case c).

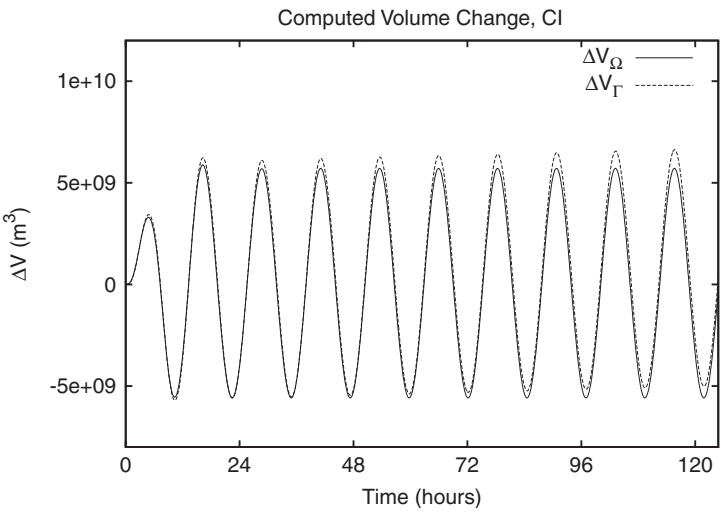

Figure 16. Volume increase calculated with the CI solution. The solid line was obtained with the domain integral of the surface-elevation term. The dashed line was obtained with the boundary integral of the flux through Γ_S (Case c).

compared with the symmetrical no Coriolis case shown in Figure 11. This is supported by Figure 16, which shows that the cumulative mass conservation error for the CI solution is reduced, compared with Case b (Figure 12). On the other hand, as shown in Figure 17, there is now a small accumulation of the mass conservation error observed for the DVBI solution.

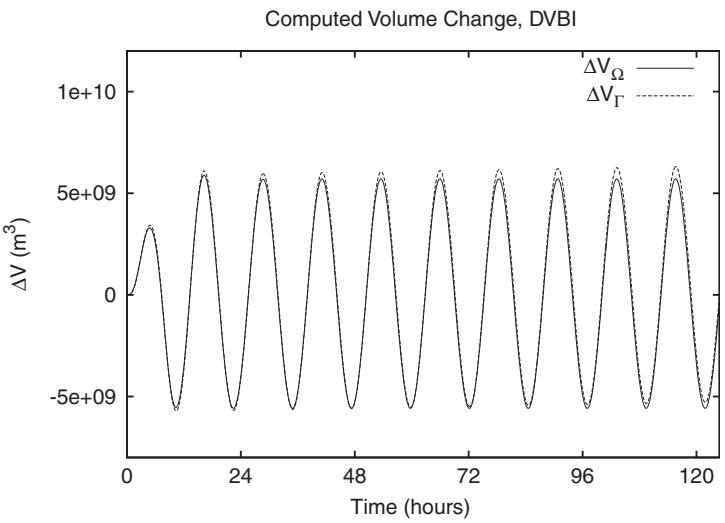

Figure 17. Volume increase calculated with the DVBI solution. The solid line was obtained with the domain integral of the surface-elevation term. The dashed line was obtained with the boundary integral of the flux through Γ_S (Case c).

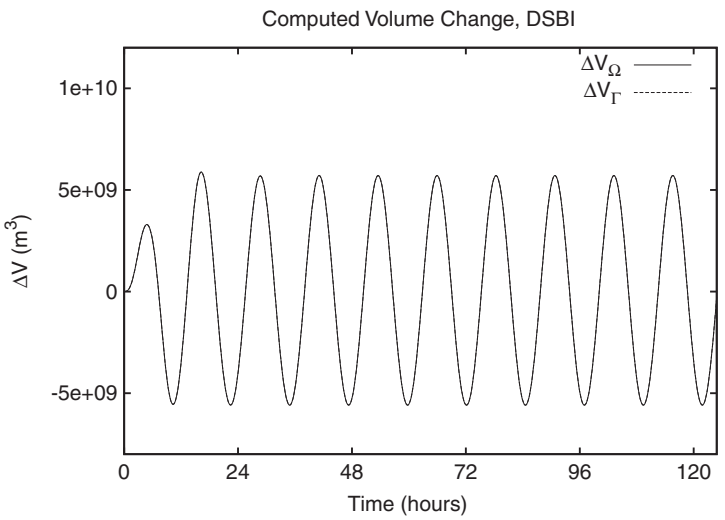

Figure 18. Volume increase calculated with the DSBI solution. The solid line was obtained with the domain integral of the surface-elevation term. The dashed line was obtained with the boundary integral of the flux through Γ_S (Case c).

This may indicate that the DVBI solution is less effective in correcting a boundary flux that is not perpendicular to Γ_S. This hypothesis is supposed by the fact that in the derivation process of the DVBI, only the normal component of velocity is modified by Equation (18). Regarding

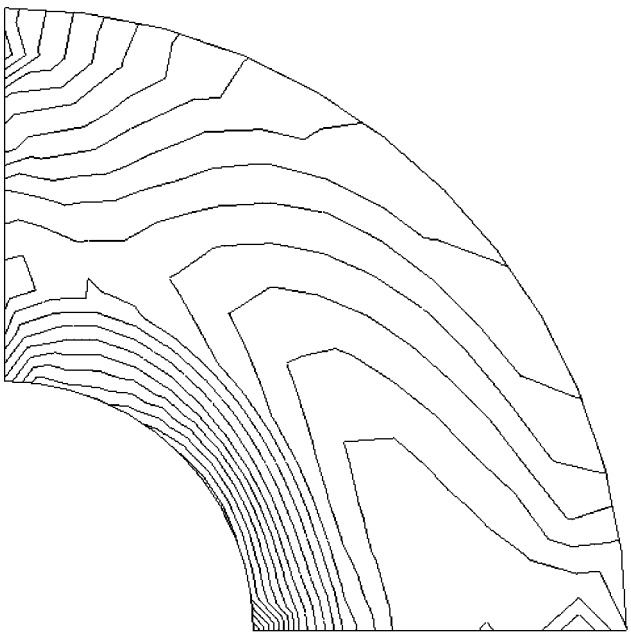

Figure 19. Distribution of the absolute value of velocity at the 32 840th time step, obtained with the CI solution (Case c).

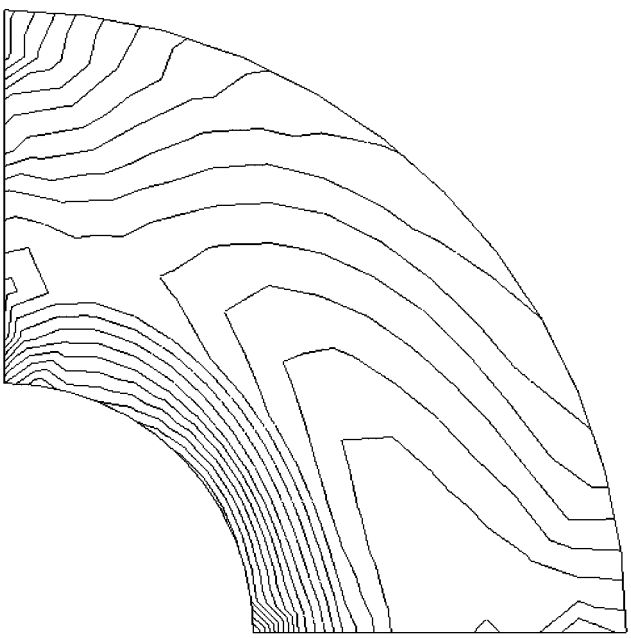

Figure 20. Distribution of the absolute value of velocity at the 32 840th time step, obtained with the DVBI solution (Case c).

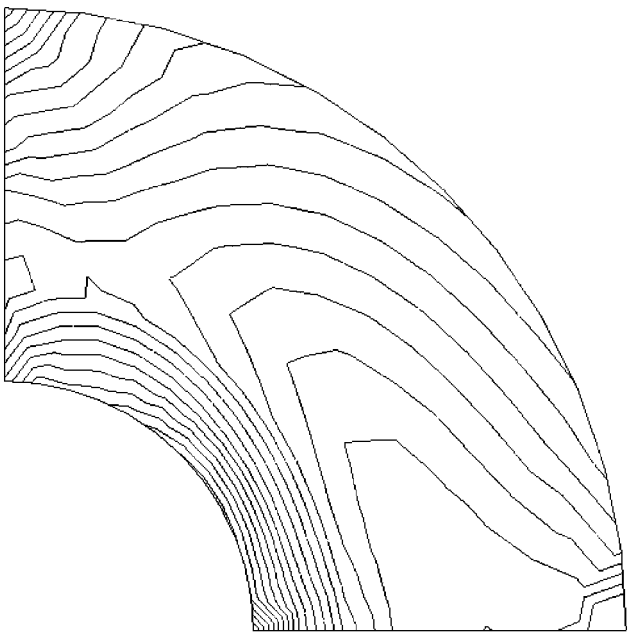

Figure 21. Distribution of the absolute value of velocity at the 32 840th time step, obtained with the DSBI solution (Case c).

the DSBI solution as shown in Figure 18, the inflow through the open boundary excellently balances with the interior volume increase.

In order to visually examine the contribution of the proposed boundary implementations, the absolute value of velocity is plotted in Figures 19, 20 and 21 using solutions obtained with the CI, DVBI and DSBI, respectively. Comparing these figures, it is observed that the DVBI improves a smoothness of the velocity solution near the open boundary, but that the DSBI yields a still smoother solution. It is clear from the precedent discussions that the proposed boundary implementations augment the accuracy of solutions, which results in the improvement of the mass conservation property.

5. CONCLUDING REMARKS

In this article, we have discussed the global mass conservation property of quasi-bubble mixed finite element formulations of the SWE. We have introduced two alternative implementations of the surface-elevation boundary condition, which are derived by applying integration by parts to some first-order spatial derivatives.

The proposed implementations, the DVBI and DSBI, were tested with numerical experiments. The results showed that both the DVBI and DSBI have a good potential to reduce the error in mass conservation through the surface-elevation Dirichlet-type boundary. The numerical experiments verified that the DSBI remarkably improves the global mass conservation property. In comparison, improvements of the DVBI seems to be limited when a flow on the

surface-elevation boundary is not perpendicular to the boundary. In terms of the jump-control term in the DSBI scheme, investigation of an adequate range of the coefficient τ_d is planned in our future work. In addition to the improvements in the mass conservation property, our preliminary numerical tests not presented here showed that both the DVBI and the DSBI improve the stability especially when there is an irregularity in the grid alignment near open boundaries in the direction normal to the boundary.

The numerical experiments demonstrated that, in order for a finite element formulation to be globally conservative, Dirichlet-type boundary conditions may need to be carefully implemented. In practical problems which involve long-term time integration or transport phenomena on the computed fluid motion, an accumulating error in mass conservation may seriously affect the reliability of solutions. Therefore, some kind of remedy such as the proposed formulations needs to be adopted to avoid such unphysical solutions.

REFERENCES

1. Hughes TJR, Engel G, Mazzei L, Larson MG. The continuous Galerkin method is locally conservative. *Journal of Computational Physics* 2000; **163**:467–488.
2. Kawahara M, Hirano H, Tsubota K, Inagaki K. Selective lumping finite element method for shallow water flow. *International Journal for Numerical Methods in Fluids* 1982; **2**:89–112.
3. Kashiyama K, Ito H, Behr M, Tezduyar T. Three-step explicit finite element computation of shallow water flow on massively parallel computer. *International Journal for Numerical Methods in Fluids* 1995; **22**:885–900.
4. Brezzi F, Bristeau MO, Franca LP, Mallet M, Rogé G. A relationship between stabilized finite element methods and the Galerkin method with bubble functions. *Computer Methods in Applied Mechanics and Engineering* 1992; **96**:117–129.
5. Franca LP, Farhat C. On the limitation of bubble functions. *Computer Methods in Applied Mechanics and Engineering* 1994; **117**:225–230.
6. Matsumoto J, Khan AA, Wang SSY, Kawahara M. Shallow water flow analysis with moving boundary technique using least-squares bubble function. *International Journal of Computational Fluid Dynamics* 2002; **16**:129–134.
7. Matsumoto J, Umetsu T, Kawahara M. Stabilized bubble function method for shallow water long wave equation. *International Journal of Computational Fluid Dynamics* 2003; **17**:319–325.
8. Westerink JJ, Gray WG. Progress in surface water modeling. *Reviews of Geophysics* (*Suppl.*). American Geophysical Union, 1991; 210–217.
9. Kolar RL, Westerink JJ. A look back at 20 years of gwc-based shallow water models. *Proceedings of the XIII International Conference on Computational Methods in Water Resources*, Calgary, Alberta, Canada, 2000; 899–906.
10. Mewis P, Holz K-P. A quasi bubble-function approach for shallow water waves. *Advances in Hydro-Science and Engineering*, vol. 1, 1993; 768–774.
11. Galland JC, Goutal N, Hervouet JM. Telemac: a new numerical model for solving the shallow water equations. *Advances in Water Resources* 1991; **14**:138–148.
12. Hervouet JM. On spurious oscillations in primitive shallow water equations. *Proceedings of the XIII International Conference on Computational Methods in Water Resources*, Calgary, Alberta, Canada, 2000; 929–936.
13. Atkinson JH, Westerink JJ, Hervouet JM. Similarities between the quasi-bubble and the generalized wave continuity equations to the shallow water equations. *International Journal for Numerical Methods in Fluids* 2004; **45**:689–714.
14. Bunya S, Westerink JJ, Yoshimura S. Discontinuous boundary implementation for the shallow water equations. *International Journal for Numerical Methods in Fluids* 2005; **47**:1451–1468.
15. Okamoto T, Kawahara M, Ioki N, Nagaoka H. Two-dimensional wave run-up analysis by selective lumping finite element method. *International Journal for Numerical Methods in Fluids* 1992; **14**:1219–1243.
16. Lynch DR, Gray WG. A wave equation model for finite element tidal computations. *Computers and Fluids* 1979; **7**:207–228.
17. Kolar RL, Gray WG, Westerink JJ. Boundary conditions in shallow water models—an alternative implementation for finite element codes. *International Journal for Numerical Methods in Fluids* 1996; **22**:603–618.
18. Zienkiewicz OC, Taylor RL, Sherwin SJ, Peiró J. On discontinuous Galerkin methods. *International Journal for Numerical Methods in Engineering* 2003; **58**:1119–1148.
19. Lynch DR, Gray WG, Analytic solutions for computer flow model testing. *Journal of the Hydraulics Division* 1978; **104**:1409–1428.

